https://doi.org/10.48047/AFJBS.6.13.2024. 956-982

African Journal of Biological Sciences

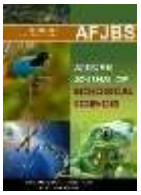

Homing Silymarin Targeted To Asialoglycoprotein Receptors On The Surface Of HepatocellularCarcinoma

Amr Sayed[1], Ahmed Nabil[1*], Islam S. Ali[2], Mariam Elwan[3], Zeinab Reyd[4], Khaled Ali Elnesr[5], Ahmed A. G. El-Shahawy[4]

[1] Biotechnology and Life Sciences Department, Faculty of Postgraduate Studies for Advanced Sciences (PSAS), Beni-Suef University, Beni-Suef, Egypt

[2] Basic Science Department, Delta University for Science and Technology, Gamasa, Dakahlia, Egypt.

[3] Egyptian Ministry of Health, Mansoura, Dakahlia, Egypt.

[4] Materials Science and Nanotechnology Department, Faculty of Postgraduate Studies for Advanced Sciences (PSAS), Beni-Suef University, 62511 Beni-Suef, Egypt.

[5] Pathology Department, Faculty of Veterinary Medicine, Beni-Suef University, Beni-Suef, Egypt.

***Corresponding author:**
Ahmed Nabil, Biotechnology and Life Sciences Department, Faculty of Postgraduate Studies for Advanced Sciences (PSAS), Beni-Suef University, Beni-Suef, Egypt,
E-mail: DRNABIL_100@hotmail.com

Tel: (+2) 01000618349

Article History
Volume 6, Issue 13, 2024
Received: 18June 2024
Accepted: 02July 2024
doi:*10.48047/AFJBS.6.13.2024.* 956-982

Abstract

Hepatocellular carcinoma (HCC) is the most common cancer and ranks third in the world in terms of cancer- related mortality. Chemotherapy is a clinical treatment for HCC. However, most anticancer medications exhibit significant toxic effects and reduced selectivity, which induce systemic toxicity. However, the targeted delivery of the drug to the liver was achieved successfully. In the current study, we designed a nanocomplex of chitosan nanoparticles loaded with silymarin that was galactosylated to target the asialoglycoprotein receptor, which is present in liver cells. The adjusted nanocomplex and its components were characterized using various techniques. An in vitro release study was performed. The study performed bioassays against HepG2 cell lines for cytotoxicity, ROS generation, flow cytometry to detect cell cycle analysis, and levels of the apoptotic markers TGF-1, Bcl-2, Cytochrome c, Caspase-3, Caspase-8, and Caspase-9. According to our results, targeted Silymarin significantly increased the expression of pro-apoptotic proteins such as p53 and caspase-3 and reduced anti-apoptotic proteins such as Bcl-2. Taken together, our results propose that the prepared nanocomplex might signify a promising tumor-targeting drug delivery system that can carry anticancer agents in a precise way to enforce HCC outcomes in the future.

Keywords: Hepatocellular carcinoma; Chitosan nanoparticles; Silymarin;

Graphical Abstract:

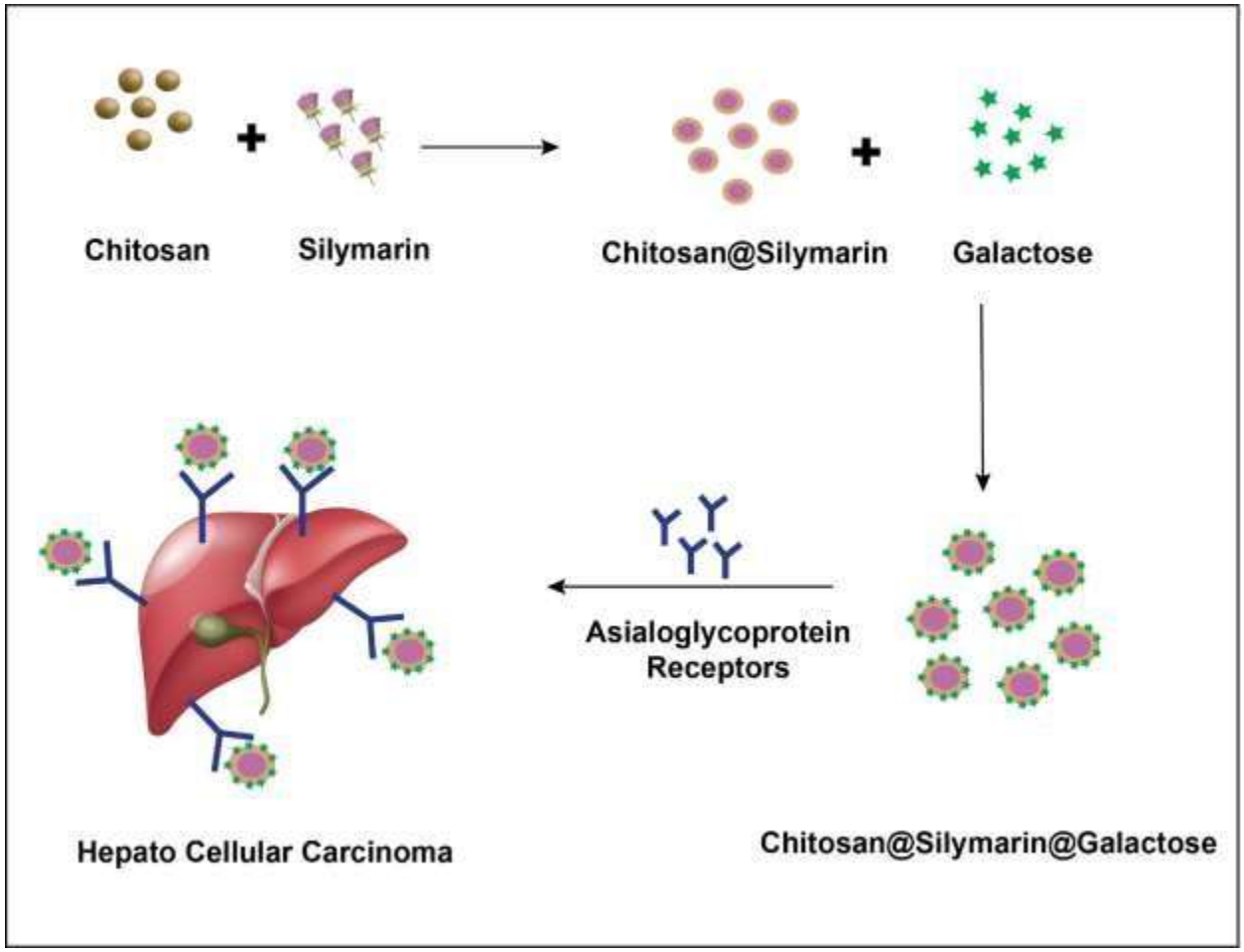

Introduction

The prognosis for HCC is poor, ranking it third among cancer-related mortality causes [1]. The main tumor markers of HCC include alpha-fetoprotein (AFP), which is a serum glycoprotein, and des-gamma-carboxy prothrombin (DCP). HCC patients do not benefit from surgical resection, as they often come in advanced stages. There are several therapeutic options for treating HCC, but chemotherapy is the most significant modality for treating advanced HCC. Chemotherapy is adopted for treating patients who were deemed inappropriate for surgical resection, localized ablative remedy, or transarterial chemoembolization (TACE), have extrahepatic metastases, exhibit evidence of vascular invasion, or are TACE-refractory [2].

However, the efficiency of chemotherapy remains below a satisfactory level and the prognosis of patients with HCC patients' prognosis remains poor [3]. One of the reasons is the relatively wide distance between the drug administration site and the site of the likely therapeutic effect. The development of cancer chemotherapies intends to expand the survival of this population [4]. Although these molecules commonly face essential difficulties, including nonselective biodistribution and reduced specificity, doxorubicin (DOX) and paclitaxel (PTX) are strong anticancer medicines. It was disappointing that PTX administration causes numerous off-target consequences such as myelosuppression, hypersensitivity-based interactions, and neurotoxicity [5].

In terms of systemic chemotherapy, Sorafenib (Nexavar®), a multikinase inhibitor, has originally been reported in HCC, and its use as a first-line treatment agent for patients with advanced HCC is now routine practice [6]. Additionally, Regorafenib has become the second treatment option for patients with advanced disease after the Sorafenib therapy [3]. Lenvatinib is also recognized as an alternative treatment for advanced HCC [7]. Deferoxamine shows great efficiency in arresting the cell cycle and inducing apoptosis, and a study was carried out using Deferoxamine in patients who have not benefited from chemotherapy for hepatic arterial infusion chemotherapy [8]. However, the demand to enhance the efficiency of chemotherapy agents is essential. Therefore, significant research has been conducted on issues related to targeted drug delivery.

Nanocarrier drug delivery techniques were the result of several interdisciplinary research efforts, including those in pharmaceutics, biology, chemistry, material science, and clinical medicine [4]. The unique properties of nanocarriers, such as their reduced size and large surface area-to-volume ratio, afford minute vehicles for carrying different compounds (eg, minute molecule drugs, proteins, RNA, DNA, and probes) with extreme efficacy [9]. Furthermore, because of the enhanced permeability and retention (EPR) impact, nanocarriers passively concentrate within the interstitial tumor because of the uneven pattern of the tumor blood vessel. However, the effectiveness of nanocarriers depends largely on the targeted delivery of drugs in close proximity to cancer cells [10].

However, an improved anticancer consequence can be assumed if the nanosized medicine is adsorbable on the surface of the malignant cell and additionally endocytosed into the tumor cell. Nanocarriers equipped with homing devices were inspected in different cancers as a malignant cell's definite recognition mechanism, similar to an active radar-guided missile to its target [11]. Furthermore, nanocarriers can limit the early release of drugs to allow adequate time for therapeutic action; this also allows the release of administered drugs to be tailored to interact with certain stimuli such as heat, light, pH, or enzymes [12]. In light of the foregoing and in response to the demand for new multifunctional materials, the overall aim of this research study is to target the HCC with a multifunctional nanocomplex. To achieve the objective, our objective was to design a nanocomplex of chitosan nanoparticles (CsNPs) loaded with silymarin that was galactosylated (CsNPs-Silymarin-galactosylated) to target the asialoglycoprotein receptor (ASGP-R) that exists over the normal hepatocyte surface and is overexpressed on the HCC cell surface. This is the novelty of this manuscript, achieving active targeting. We hypothesized hydrogen bond formation due to a reaction among the hydroxyl groups of the terminal galactose sugar or the protonated amino group of chitosan and the carbohydrate recognition domain (CRD) of the ASGP-R, which is found on the extracellular side, and the cellular uptake of the nanocomplex may be endocytosed via clathrin-coated pits. In light of the results obtained, it has been thought that the designed material meets the requirements for HCC treatment. However, more animal studies are required to implement the data obtained in clinical science.

1. Experimental:

1.1. Materials

N-hydroxyl succinamide (NHS), N, N'-dicyclohexyl carbidimide (NNDCHC), and glacial acetic acid were purchased from Loba Chemistry Pvt. Ltd., India. Silymarin was supplied by Sigma-Aldrich, Belgium. Chitosan, tripolyphosphate (TPP) and galactose were purchased from Vikaash Chemicals, India. The glutaraldehyde solution was purchased from ADVENT Chembio Pvt. Ltd., India. Other solvents used were obtained from commercial stores with a high purity level.

1.2. Synthesizing GLPs-CsNPs-Silvermarin nanocomplex

Chitosan nanoparticles have been prepared by the ionotropic gelation method as described [13]. In summary, 0.4 g of chitosan powder was placed in 200 ml of distilled water with magnetic stirring for 10 minutes, followed by 2 ml of a 1% glacial acetic acid solution. The PH of the solution reached 5 by adding 1 M NaOH dropwise with vigorous stirring for 20 minutes. The TPP solution was then added dropwise to the mixture in a 4:1 ratio (Chitosan: TPP) ratio and stirred for 5 minutes, forming mixture 1. A Silymarin loading was conducted as follows: To mixture 1, 0.04 g of silymarin, which was previously dissolved in 2 ml of methanol, was added, forming mixture 2, which was transferred to a probe sonicator for 15 min. The coupling with galactose was preceded as follows: A mixture 3 consisting of 0.25 g of sodium acetate, 40 ml of distilled water, 0.5 g of galactose powder, 0.25 g of dicyclohexyl carbidimide and 0.25 g of N-hydroxyl succinamide was prepared and added dropwise to mixture 2 with continued sonication for 20 min, forming mixture 4. This solution was retained at room temperature with dynamic stirring for 72 hours. Subsequently,

8 ml of 2% glutaraldehyde as a crosslinking agent and 5% D-mannitol were added to the solution, which was then stirred for 6 h. Finally, the mixture was lyophilized and freeze-dried.

1.3. Characterizations

1.3.1. X-ray diffraction (XRD)

The XRD method was used to assess the crystallinity of the materials using Cu K radiation (λ = 1.54 nm). The device has been programmed to work at a current of 30 mA and an operating voltage of 40 kV (power 1200 W) with a scan speed of 2 degrees per minute (step size equals 0.050 degree; step time equals 1.5 s) and a scanning range of 2 theta angles (10o to 50o). Through the International Centre for Diffraction Data Cards, we identified the crystallinity phases. Applying Scherrer's equation $D = 0.94\lambda/\beta \cos \theta$ (Eq. 1), XRD peaks were utilized to calculate the size of the crystallite, since D refers to the mean crystallite size, λ denotes the radiation wavelength, β represents the designed entire width at half the maximum of the diffraction peak, and θ accounts for the diffraction angle of Bragg.

1.3.2. Fourier transformation infrared spectroscopy (FTIR)

FTIR of 4500–500 cm^{-1} has been adopted for recognizing the functional groups. A Bruker (Vertex 70 FTIR-FT Raman) spectrometer was employed to collect FTIR spectra. The prepared formula spectra were combined. The scanning resolution was adjusted to 1 cm^{-1}, and the average of the spectra was taken after three scans.

1.3.3. Morphology Investigation

The particle size and surface morphology of the manufactured formula were evaluated by scanning with a high-resolution TEM (HRTEM, JEM 1400, software version DM_3, Japan) adjusted at a voltage of 300 kV. A field emission scanning electron microscope (FESEM; Philips XL30 instrument, The Netherlands) was also incorporated into this assessment. The samples were initially subjected to diffusion in deionized water and diluted at 1:5 (v/v) at room temperature.

1.3.4. Measurements of Zetasizer and Zeta Potential

The polydispersity index value, zeta potential, colloidal stability, and hydrodynamic size of the dispersed formula have been computed with the photon correlation spectroscope or dynamic light scattering (DLS) of the ZS90 Zetasizer instrument (Malvern, United Kingdom). By means of distilled water, the sample volume (1 ml) incorporated in the analysis was kept unchanged. Particle Brownian motion induces light intensity scattering from particles, which is then sensed as an intensity variation via a suitable photomultiplier and optics. The potential diversity of zeta was assessed within a distilled water dispersant having a 1.330 refractive index [14]. All data investigations were performed in automatic mode, with three readings for each run.

1.3.5. UV-vis spectra

UV spectrophotometry represents an analytical method normally designated for qualitative and quantitative evaluations because of its low cost and consistency. The UV-vis spectrometer (CARY100, Germany) was used to calculate the loading effectiveness of galactosylated chitosan nanoparticles loaded with silymarin, and the percentage

of Silymarin release was calculated at the Silymarin absorption peak, which had a single conspicuous peak (λ max) at 287 nm [15].

1.3.6. Entrapment Efficiency

To judge silymarin entrapment efficiency (EE%), the CsNPs-Silymarin galactosylated formula was left in a centrifuge (at 14,000 rpm and 4°C) and operated for a period of 45 minutes to isolate the supernatant comprising free silymarin. A UV-vis spectrophotometer was utilized to calculate the amount of free silymarin at λ max = 287 nm. Measurements were made in triplicate (n = 3). EE% has been assessed from the following equation:

$$\text{EE\%} = \frac{total\ silymarin - \ free\ silymarin}{total\ silymarin} x100\ (Eq.2)$$

1.3.7. Silymarin Release Study

The release of silymarin from the CsNPs-Silymarin-galactosylated formula was quantified using a modified dialysis bag technique [16]. The initial mass of CsNPs-Silymarin-galactosylated silymarin for release was 0.1 gm, involving the corresponding mass of 20 mg of silymarin. The loading capacity (LC%) and entrapment efficiency (EE%) percentages were computed depending on the following equations [17].

$$\%LC = \frac{\text{Initial silymarin} - \text{Free silymarin}}{\text{galactosylated} - \text{CsNPs} - \text{silymarin}}\ X100\ \ (Eq.3).$$

$$\text{EE\%} = \frac{Total\ amount\ of\ drug\ added - amount\ of\ free\ drug}{Total\ amount\ of\ drug\ added}\ \ (Eq.4)$$

In conclusion, 5 ml of CsNP-Silymarin-galactosylated suspension (comparable to 20 mg of silymarin) was placed in a dialysis bag (cellophane membrane, molecular weight cutoff at 10,000–12,000 Dalton), which was placed within a 200 ml phosphate buffer (pH 6.8). Dialysis was achieved in a shaking incubator adjusted at a temperature of 37 ° C and 150 rpm. The samples were removed and replaced by a new buffer at different time intervals. A spectrophotometer was adopted to measure silymarin concentration at a maximum of 287 nm. The free silymarin liberated under the same circumstances was also evaluated as a control. Each measurement has been repeated three times.

1.3.8. Kinetics release of silymarin from galactosylated- CsNPs- silymarin formula

Data derived from the release examination were analyzed using kinetic models (eg, zero order, first order, Korsmeyer-Peppas, Higuchi and Hixson). The correlation coefficients (R^2) were adjusted to the best-fitting model. The mechanism of drug release was defined from the Peppas equation as follows:

$$\frac{Mt}{M\infty} = \text{Kt}^n\ \ (Eq.5)$$

Where Mt denotes the amount of drug released during time t, M refers to the total amount of drug released at infinity, K represents the rate of release constant, and "n" marks Peppa's diffusion exponent, demonstrating the drug release method and the kind of diffusion [18].

1.4. Bioassays:

1.4.1. Cytotoxicity in vitro assay

Cytotoxicity of the CsNPs-Silymarin-galactosylated formula was investigated against mammalian cell lines: MRC-5 cells (normal human lung fibroblast cells) and HepG2 cell lines. Cell lines were obtained from the Holding Company for Biological Products and Vaccines (VACSERA), Giza, Egypt's tissue culture unit. We compared the cytotoxicity of the formula with that of 5-fluorouracil (5-FU) as a reference anticancer agent. Cell viability was established *in vitro* via the 3-(4, 5-dimethylthiazol)-2-diphenyltetrazolium bromide (MTT) assay. Cells were cultured in a 96-well plate for 48 hours with dimethyl sulfoxide (DMSO 0.5%) and left for 6 hours to starve, and then treated by serial dilutions of the tested formula in the cell medium [19]. After 48 hours of incubation at a specific concentration of 0.5 mg / ml, MTT was supplied for all wells and again left for incubation for an additional 4 hours. Subsequently, the solution was removed and DMSO (150 μL) was supplied for all wells prior to optical density absorbance measurement at 590 nm by the microplate reader (Bio-Rad Model 680, Hercules, CA, USA) to define the number of viable cells and the percent of viability [(ODt / ODc)] x 100%. The ODt denotes the mean optical density of wells treated with tested sample, and the ODc denotes the mean optical density of untreated cells. The inhibitory concentration (IC50), which is the concentration demanded to induce toxicity within half of the intact cell, has been evaluated. Cytotoxicity was calculated as a percentage of cell viability. The test was performed with measurements made in triplicate. Furthermore, Cytotoxicity of the CsNPs-Silymarin-galactosylated formula was incubated with HepG2 cell lines for 48 h, and its cellular uptake was examined using a JEOL JEM 1010 TEM at 70 kV at Al-Azhar University's Regional Center for Mycology and Biotechnology (RCMB).

1.4.2. Flow Cytometry Assay

To delineate the impact of the tested formula on the distribution of the cell cycle within HepG2 cell lines, we performed the cell cycle investigation using the Cycle TESTTM PLUS DNA Reagent Kit (Becton Dickinson Immunocytometry Systems, San Jose, CA). HepG2 cells were stained with propidium iodide according to the technique offered through the kit and subsequently performed on the cytometer. The distribution of cell cycles was estimated by CELLQUEST software (Becton Dickinson Immunocytometry Systems, San Jose, CA) [20]. Additionally, the levels of apoptotic markers of Bcl-2, TGF-beta1, Caspase-9, Caspase-3 and Cytochrome c were evaluated using a flow cytometric assay. During the flow cytometry assay, we investigated a population of HepG2 cells with 10^7 events to obtain a sufficient number of cells for statistically significant detection.

1.4.3. ROS generation assay

According to [21], the generation of ROS in the treated HepG2 cells with the tested formula was estimated using 2-7 dichlorofluorescein diacetate (DCFDA) dye. In summary, PC-3 cells (1 104 cells/100 l) have been dispersed

in 96-well black bottom plates, left to incubate for 24 hours, and exposed to the formula (at IC50 concentration) for 24 hours. Subsequently, we washed the cells with PBS and incubated them with DCFDA dye (20 M in PBS) at 37 ° C for 30 min. The dye solution was then replaced with 200 liters of PBS. Fluorescence emission was measured at 528 nm in a multi-well plate reader (SYNERGYHT, Biotek, USA) using KC-4 software. The data obtained have been presented as ROS generation percentiles relative to unprocessed HepG2 cells.

1.4.4. Estimation of Cytochrome c release:

We delineated the cytochrome c release using the Cytochrome c ELISA Assay Kit (Cat.KHO1051, Thermo Fisher Scientific). 100 µl of mitochondrial extracts were added to the microplate well and layered with a monoclonal antibody directed against cytochrome c. Then a biotin-conjugated solution was added for 2 hours at room temperature (RT). A working solution of streptavidin-HRP was loaded into the wells after washing and left for 1 hr for incubation at RT. Tetramethylbenzidine solutions were loaded into the wells and left to incubate in a darkened condition for 15 minutes in RT. After adding the stop mixture, the absorbance was assessed at 450 nm [22].

1.5. Statistical analysis

The data was coded and entered using the SPSS version 22 statistical package. Data were summarized using the mean and standard deviation. The data were explored for normality using the Kolmogorov-Smirnov test. Comparisons of different outcomes for normally distributed data were performed using the ANOVA test; A P value less than or equal to 0.05 will be considered statistically significant. All tests will be two-tailed [23].

2. Results and discussion:

2.1. Qualitative analysis of XRD

The XRD patterns of Chitosan, Chitosan-NPs, Silymarin, Galactose, and CsNPs-Silymarin-galactosylated are illustrated in Fig. 1. The Chitosan XRD spectrum reveals lowered intensities of the diffraction signal, suggesting reduced chitosan crystallinity. The decrease in crystallite size was demonstrated by the expanded width of the diffracted peaks. Based on Eq. 1, the pure chitosan crystallite attained 2.98442 in size. The XRD spectrum of CsNPs exhibits a disordered alignment of chitosan chains, displaying an expanded diffuse hump peak at around 20 ° (that is, the characteristic semicrystalline chitosan fingerprint). The findings of the current study agreed with the results of an earlier study [22], which verified that the TPP counterions persuade cross-linkage amongst chitosan chains, leading to the construction of an opaque network that vanishes the chitosan diffraction peaks, establishing a single floppy peak. In contrast, the presence of a wide peak designated a decrease in crystallite size, indicating less periodicity (i.e., long-range order of ions, atoms, or molecules within the particles), and hence lowered hkl planes ordering, i.e., a crystallinity decline [24]. An additional probable explanation for the reduced degree of crystalline perfection was crystal nucleation and growth rate defects triggered by the use of a polymer like chitosan [25].

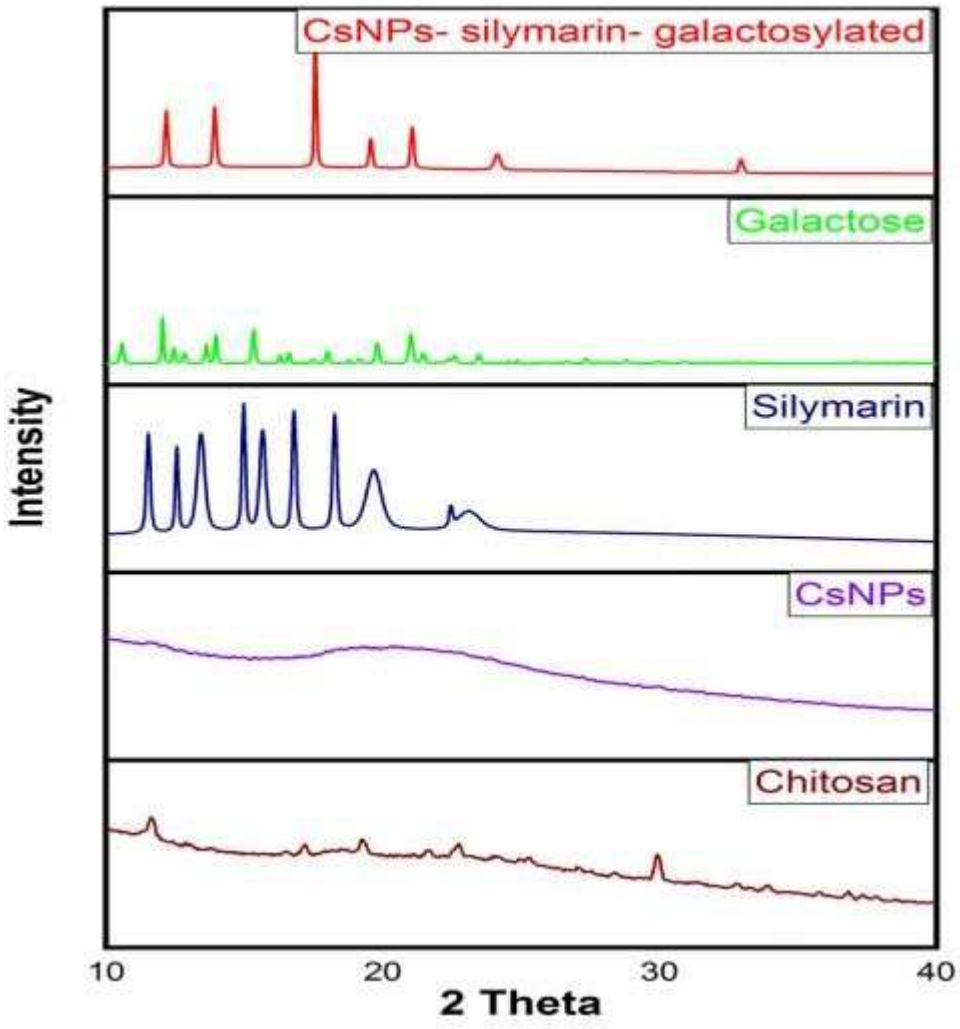

Fig.1. The XRD of chitosan, CsNPs, silymarin, galactose, and CsNPs-silymarin-galactosylated, revealing variations in the peak position, width, and intensities among the investigated entities

The Silymarin crystal structure was determined using powder X-ray diffraction to improve our understanding of the chemical action of Silymarin. The figure covers an abundance of diffracted peaks, indicating multiple structural plans and the prevalent electron densities of its chemical formula, $C_{25}H_{22}O_{10}$. The elevated signal intensity with thin diffracted peaks denotes an enhanced crystallinity state. In other words, these diffraction peaks were retained in the physical mixture, suggesting that silymarin remained in a crystalline state. No splitting in the peaks ends up endorsing a single phase of silymarin. The XRD spectrum obtained from silymarin in the previous study demonstrated a peak with a relative intensity of 100% and a d space of 4.48884 at 19.7786^{o} [2 θ]. The low signal intensities just existed within the spectrum due to the overlap between Bragg peaks. Galactose is a monosaccharide sugar that reveals

decreased diffraction signal intensities, signifying a decrease in crystallinity. The main peaks belonged to galactose and were located at 2, equal to 10.34, 12.78, 14.14, 15.54, 18.66, 19.74, 21.82 and 24.18.

The CsNP-Silymarin-galactosylated crystal form was shown in the same figure, showing the crystallinity of the prepared formula. The diffraction peaks hardly mimic those of silymarin, with a small right peak shift and a variation in the signal intensity. The diffracted peak repositioning may be triggered by substitution doping, stress, and temperature [26]. The shift in the peak position may result from fluctuations in the interaction angle induced by variations in structural design occurring during the loading process. Interatomic distance variations of the silymarin-CsNPs may likely cause the detected shift in the diffracted peak position. Furthermore, silymarin encapsulation inside CsNPs and silymarin intercalation with CsNPs produced planar alignment and variances in the interatomic distances. We proposed that the amino group of chitosan (NH_2) and the carbonyl groups C = O of Galactose and silymarin are chemically bonded. The absence of the silymarin diffracted peak further supports this idea. In addition, the shifting could be due either to silymarin adsorption on the surface of the CsNPs or the encapsulation operation. In total, the CsNP-Silymarin-galactosylated spectra exhibited languid variations with respect to the position and shape of the diffracted signals, in addition to the combined intensities of the diffracted peaks in a two-angle range compared to the individual entities of chitosan, CsNPs, silymarin, and galactose. These changes indicated that silymarin was loaded on CsNPs and linked to galactose.

2.2. FTIR spectra analysis

The FTIR spectra of chitosan and chitosan-NPs as precursors are presented in Figure 2. Regarding the chemical structure, the broad peak at 3419 cm^{-1} coincides with the overlapping of the N-H and O-H groups. The displayed peaks were 2924 and 2925] cm^{-1} for aliphatic C-H stretching, 1637 cm^{-1} for bending vibration of in-plane N-H, 1414 cm^{-1} for C-O primary alcoholic HC stretching vibration, and 1099 cm^{-1} for stretching vibration of C3-OH hydroxyl group [27]. The two spectra of Cs and CsNPs were relatively similar and exhibited several distinctive peaks with a minor difference in width and an insignificant shift in the position of the peak. The wide difference between chitosan and chitosan-NP could be due to the formation of hydrogen bond formation [28]. The spectrum of pure silymarin shows the following peaks: a broad band of OH groups at 3432 cm^{-1}, -C-H stretching at 2932 cm^{-1}, -C=C- stretching vibration of symmetrical aromatic ring (C=C ring) at 1504 cm^{-1}, -O-H stretch at 1069, 1159, and 1272 cm^{-1}, and -COOH carboxylic acid at 1717 cm^{-1}, indicating that the above IR spectra were of silymarin. The FTIR spectrum of silymarin obtained was well matched with that of Irfan et al. [29].

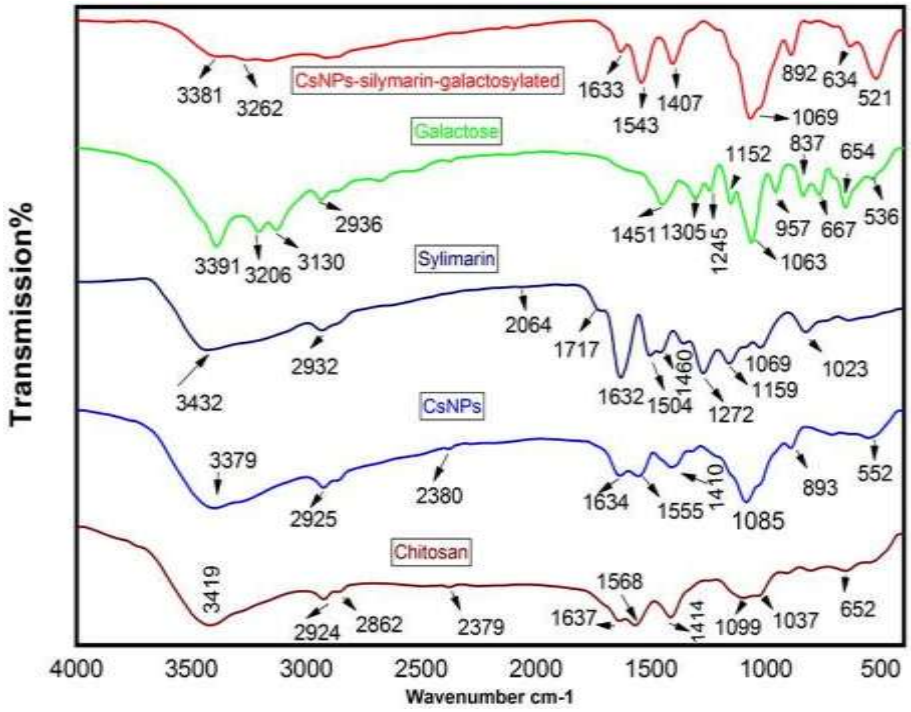

Fig. 2. The FTIR of chitosan, CsNPs, silymarin, galactose, and CsNP-silymarin-galactosylated. The lack of complex peaks of silymarin designates a successful loading within the chitosan polymeric matrix.

In agreement with Gatard et al. [30], the FTIR spectrum shows the characteristic hydroxyl group of pure D-galactose at 3391 cm^{-1}, 3206 cm^{-1}, 3130 cm^{-1}, and 2936 cm^{-1} assigned as being indicative of CH_3 stretching. Two absorption bands assigned to the O-CH bond appear at 1451 cm^{-1} and 1305 cm^{-1}. The spectral area from 1245 to 667 cm^{-1} exhibits a complex series of peaks owing largely to the CO bond. The FTIR spectra of the CsNPs-silymarin-galactosylated formula displayed peaks at 1543 cm^{-1} and 1407 cm^{-1}, reflecting N-H/C-H stretching, C=C aromatics, and the wagging of CH2 attached to chitosan OH groups. The broad peak in the range from 3381 to 3262 cm^{-1} indicates hydrogen bond formation among the OH groups of silymarin and chitosan. The lack of complex silymarin peaks designated successful loading within the chitosan polymeric matrix; further, the presence of the distinctive peak of D-galactose confirmed the labeling with galactose.

2.3. Surface morphology (HRTEM study)

We inspected the surface morphology of our synthesized nanomaterials using HRTEM. Fig. 3 shows the Silymarin and CsNP-Silymarin galactosylated HRTEM images, Figures 3A and 3B, respectively. The figures revealed nonaggregated semispherical and spherical shapes of the synthesized silymarin, with particle sizes averaging around 132.5 nm and presenting a heterogeneous morphology with an irregular particle size distribution. It should be mentioned that chitosan and silymarin contain various chemical bonds, including ionic bonds, peptide bonds, covalent bonds, hydrogen bonds, and electrostatic interaction bonds [31], which might favour their robust attachment. These

characteristic chemical interactions afford several advantageous criteria, including increased stability, high capacity, improved bioavailability, good storage, and controlled release. Fig. 3C&D is an HRTEM with a low field of view, revealing clusters of synthesized CsNPs-Silymarin. Additionally, the images displayed two varied signal intensities (arrow heads), which might be attributed to the fluctuating attenuation of the incident electron beams over CsNPs-Silymarin. This attenuation depends upon the electron densities of silymarin and chitosan NPs, which approve the loading operation. The occurrence of dark signals in particle-HRTEM images specifies the existence of flavonoids such as silymarin that are obstructed in a matrix composed of Cs polymer and polyanion TPP to compose a composite network similar to that of chamomile flowers (bright signal). The formation of silymarin-CsNPs may occur via intermolecular linkages between silymarin hydroxyl groups and amino groups of chitosan during the process of polymerization or through electrostatic reactions between cationic and anionic molecules, such as CS and silymarin molecules, respectively. This behavior was governed by the chemical and physical criteria of chitosan cargo molecules and silymarin.

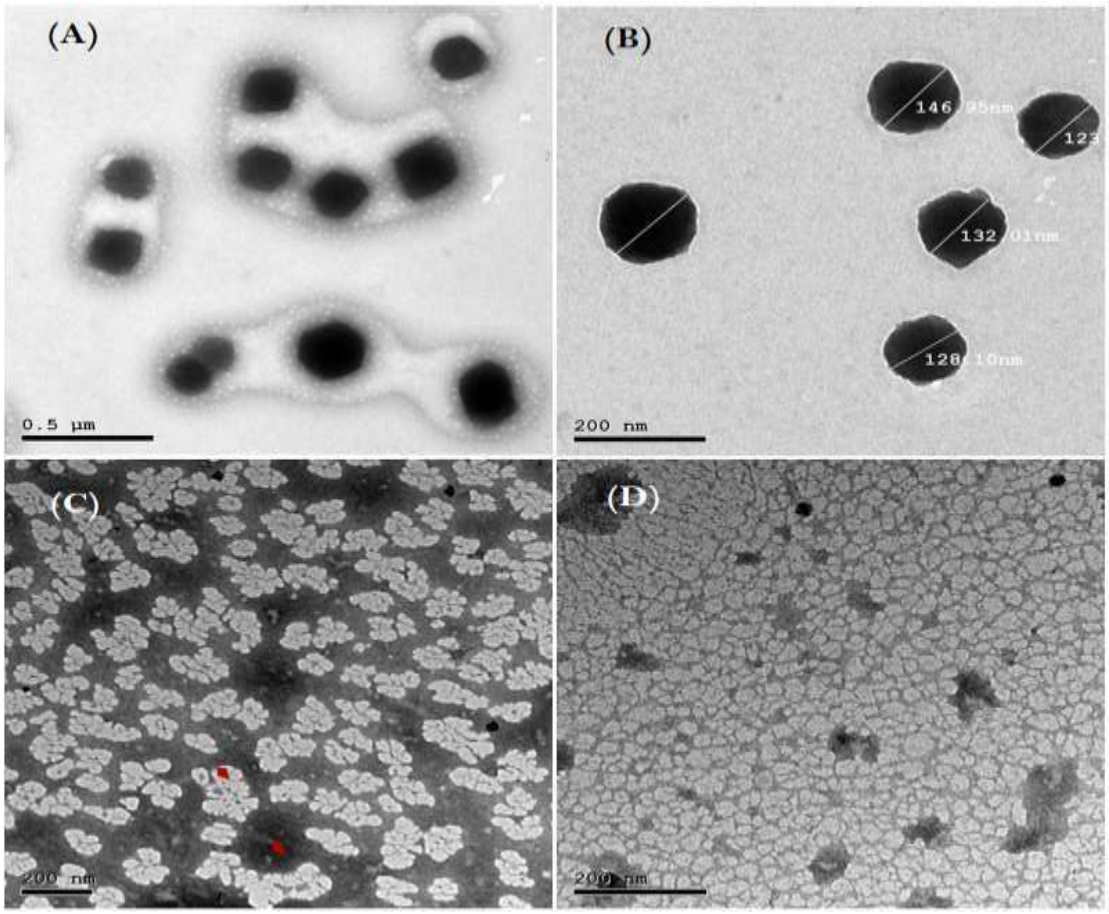

Fig. 3. HRTEM images of silymarin (A) and CsNP-silymarin-galactosylated (B), revealing nonaggregated semispherical and spherical shapes. C&D images with a low field of view display clusters of the synthesized CsNPs-silymarin.

2.4. Zetasizer and Zeta potential measurements

Dynamic light scattering (DLS) stands for the widely used methodology for measuring the size of the dispersed particles (particularly the hydrodynamic diameter) by directly measuring the translational diffusion coefficient in the continuing phase. The Z-average size (or mean), also called the cumulant mean (or "harmonic intensity averaged particle diameter"), represents the meaningful reported reading when used in a quality control set, as it was presented in ISO 13321. This designates the hydrodynamic parameter, and it is appropriate only in the case of molecules in solution or particles in dispersion. The Z-average mean size has sensitivity to even minor variations in the sample and is applicable for comparing with the size estimated via other methods if your sample is unimodal, very narrow, spherical or subspherical in shape, and prepared in an appropriate dispersant [32].

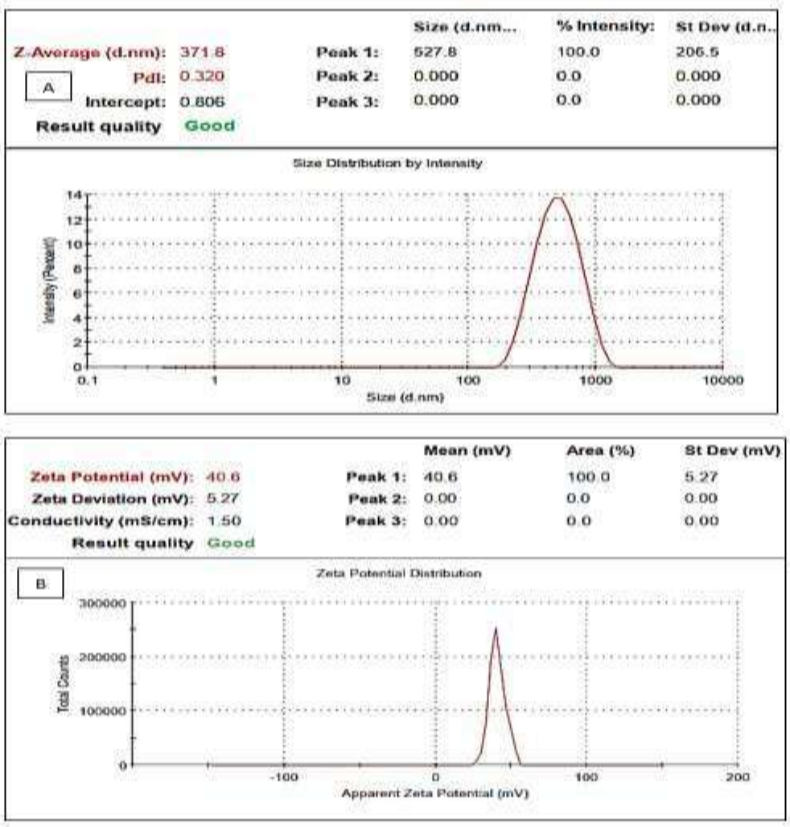

Fig. 4. Hydrodynamic diameter (A) and zeta potential (B) of CsNPs-silymarin-galactosylated. The hydrodynamic diameter average measured via DLS records a 371.8 d. nm. The zeta potential value of +40.6 mV, reflecting high stability of the complex.

Fig. 4A from the present research demonstrates the size distribution pattern exhibited by the CsNP-Silymarin galactosylated intensity. The intensity distribution is comparable in size to the cumulant fit. The sample was unimodal (i.e., revealing only a single peak) with a spherical or subspherical shape. The galactosylated CsNPs-Silymarin was measured by DLS and recorded a Z average of 371.8 d. nm, which slightly exceeds HRTEM values. This is a satisfactory result, as the number of distributions (obtained from electron microscopy) was greatly reduced compared

to that of the intensity distribution derived from DLS. In another sense, the DLS delineates the hydrodynamic diameter of the particle, but the HRTEM specifies the factual diameter of the particle. The value of the polydispersity index (PDI) ranges from 0 to 1. The value obtained (PDI = 0.320) indicated the mid-width of the peak and a diverse size distribution, which has been endorsed by the HRTEM images. The intercept value (0.806) specified an improved signal-to-noise ratio. The zeta potential has been employed primarily to inspect the surface charge and physical stability of the nanocapsules. The zeta potential values exceeding +30 mV or below -30 mV represent the reference value, which affords an adequate repulsive force to eradicate particle aggregation [33]. Repulsion amongst CsNPs-Silymarin-galactosylated suggested an elevated zeta potential value of +40.6 mV (Fig. 4B), which was greatly agreed with Ameya [34], who previously recognized carboxymethyl hexanoyl Cs with an equivalent zeta potential and elevated protein carrier stability.

2.5. Charge capacity, capture efficiency, release profile, and cytotoxicity assay:

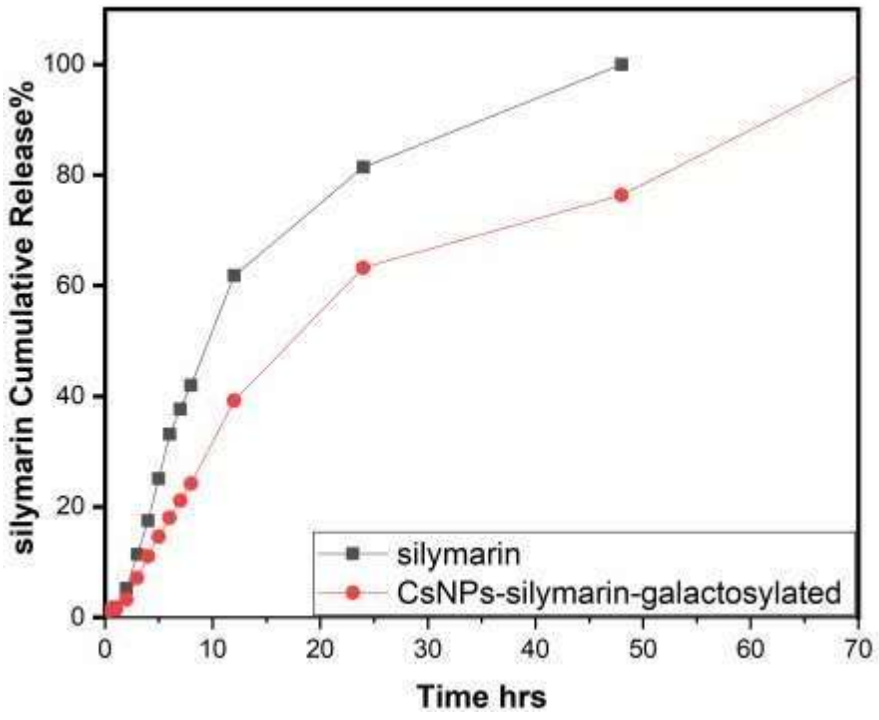

Fig. 5. Release profile of free silymarin and silymarin from the CsNPs-silymarin-galactosylated formula in PBS solution, demonstrating that the free silymarin had a minor cumulative drug percentage compared to the CsNPs-silymarin-galactosylated formula, suggesting a sustainable release pattern.

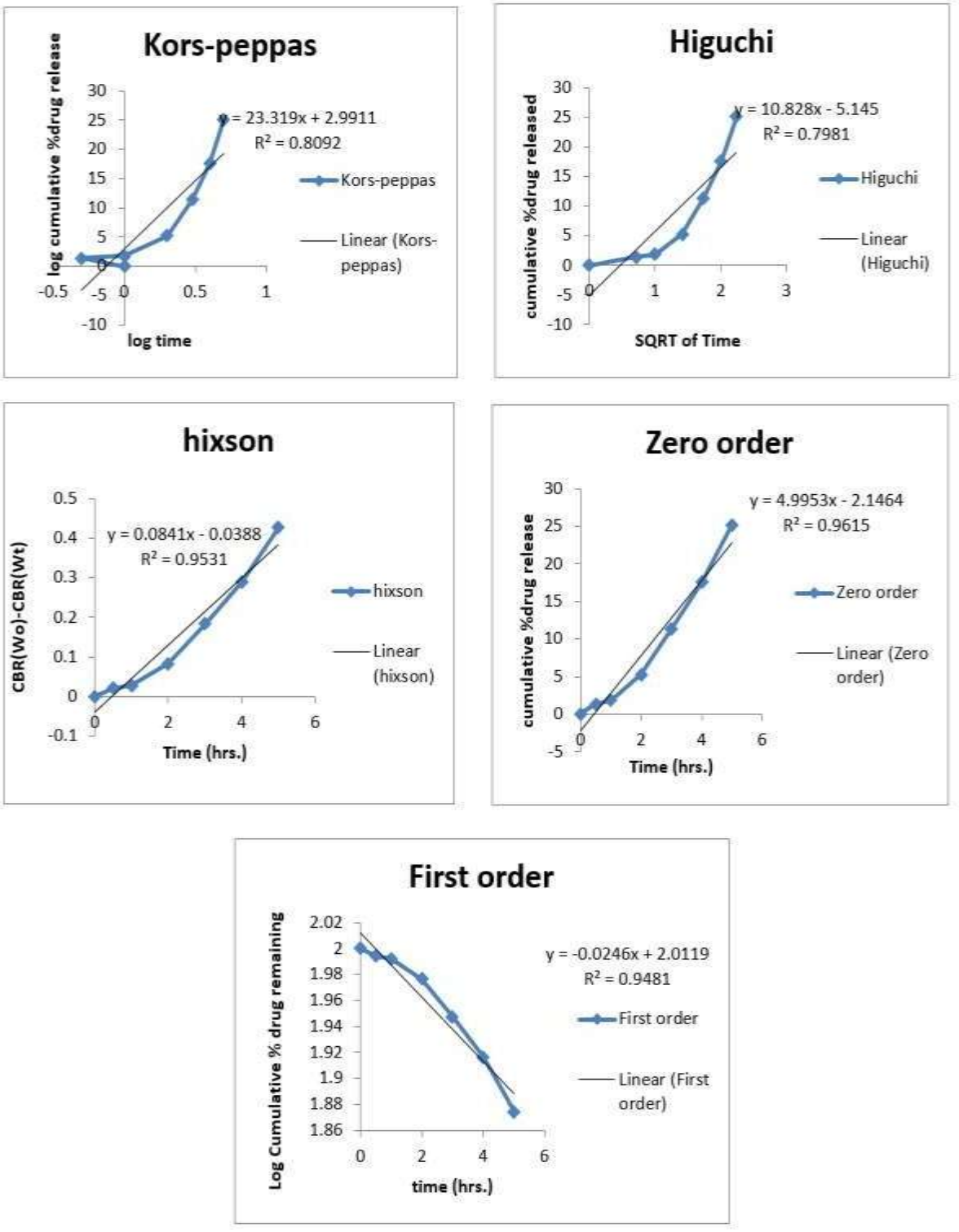

Fig. 6. Kinetic silymarin release data according to the zero-order equation, the first-order equation, Korsmeyer-Peppas, Hixson-Crowell and Higuchi. The silymarin was released using diffusion with a highly best-fitting zero-order.

The LC denotes the drug quantity associated with the unit weight of the formula. Using Equations 3 and 4, the results showed that the LC% was 29% and the EE% was 84%. Fig. 5 shows the 72-hour release profile of free silymarin and silymarin from the CsNPs-Silymarin galactosylated formula in PBS solution at unchanged pH (6.8) and temperature (37°C). The silymarin revealed two stages of release: a comparatively quick burst release stage succeeded with a distinctive slow release rate that lasted up to 45 hrs in free silymarin, while the formula lasted up to 72 hrs, signifying a continuous release model. Free silymarin exhibited a burst release of 20± 2.5% in approximately 2 h, while the burst release time in the formula was 6 h with the same percent. Free silymarin is released more rapidly than CsNPs-silicomatosylated. This could be induced by the occurrence of silymarin deeper within the CsNPs matrix. The early fast release of the transported silymarin could be explained by silymarin scattering over the surface of CsNPs, where silymarin could continuously release out of the CsNP core in response to chitosan swelling and hydration. Free silymarin had a minor cumulative drug percentage compared to that of CsNPs-Silymarin galactosylated CsNP, which is attributable to the slow diffusion of silymarin from the chitosan-NPs matrix. After 40 h, the saturated percent of cumulative free silymarin release attained approximately 80%, while CsNPs-silymarin galactosylated exposed a continued release pattern of 90% up to 72 h. In this research, we conducted a release kinetic experiment to delineate the release order. The kinetic examination of the released silymarin from CsNPs-silymarin-galactosylated was conducted. Kinetic Silymarin release data were fitted according to four equations as follows: zero order equation, first order equation, Hixson-Crowell, Korsmeyer-Peppas, and Higuchi, as shown in Fig. 6. The mechanism of silymarin release was related to the kinetic model with a high correlation coefficient score (R^2). The release of silymarin was accomplished through diffusion with a highly best-fitting zero order.

2.6. Bioassays:

2.6.1. Cytotoxicity activity (IC 50):

In terms of the cytotoxicity assay, the cytotoxic issues of the materials are crucial to their medicinal implications. Again, in the current study, we used the MTT test to evaluate the cytotoxicity of silymarin, CsNP, CsNPs-silymarin, CsNPs-silymarin galactosylated silymarin and 5 F U versus the HepG2 cell line. In Table 1, we found that a dose of silymarin between 750 and 1000 μM was needed to kill half of the cancer cells. The estimated IC50 value was 1500 μM in the group of silymarin nanoparticles loaded with chitosan, while the dose was less than 250 μM in the group of CsNP-Silymarin galactosylated. When 5-fluorouracil (5-FU) was used as an approved comparative drug, its IC50 value was 100 μM. The chitosan dose was only 1000 μM, and galactose stimulated HepG2 cell proliferation. Table 2 shows a comparison of CsNPs-Silymarin-galactosylated and 5-FU in normal cell lines HepG2 and MRC-5. The dose of the CsNPs-Silymarin-galactosylated group in the HepG2 cell line was <250 μM, and was 750 μM in the normal cell line MRC-S. The value of the selectivity index was 3. This means that we needed <250 μM of CsNPs-Silymarin galactosylated to kill 50% of the HepG2 cell line, while in MRC-5 we needed three times the effective dose used in the HepG2 cell line. Furthermore, 5-FU IC50 concentrations on the HepG2 cell line and the normal MRC-5 cell line were 100 M and 180 M, respectively. The selectivity index of 5-FU was 1.8. Selectivity values alone indicated that the CsNPs-Silymarin galactosylated group was safe.

Table 1. IC50 concentration in silymarin, silymarin loaded with chitosan, galactosylated silymarin loaded with galactosan, chitosan, galactose, and 5-FU:

Treatment	IC_{50} concentration against Hepg2 cell line
Silymarin	750-1000 μM
Silymarin + chitosan	1500 μM
Silymarin + chitosan + gala	< 250 μM
Chitosan	1000 μM
Galactose	Galactose stimulates the proliferation of HepG2 cell line
5 F U	100 μM

Table 2. IC50 concentration in HepG2 cell line and MRC-5 normal cell line and selectivity index between treated groups galactosylated chitosan-loaded silymarin, and 5-FU:

Treatment	IC_{50} concentration against Hepg2 cell line	IC_{50} concentration against MRC-5 normal cell line	SI
Silymarin + chitosan+ galactose	<250 μM	750 μM	3
5 F U	100 μM	180 μM	1.8

In a study, silymarin, tested alone or with other substances, was recognized to reduce the telomerase activity of different types of cancer cells, and telomerase activation is among the initial HCC events. It accounts for one of the steps adopted to limit the rate of initiation and prognosis of hepatocarcinogenesis. In fact, more than 85% of patients exhibit elevated telomerase enzyme activity, where the diameters of the telomere vary from neighboring cells [35]. Furthermore, the effect of chitosan on the same carcinoma has been studied, and chitosan showed a protective outcome on HepG2 cell proliferation and inhibited tumour growth [36]. Similarly, Azuma et al. considered chitosan a promising antitumor drug against hepatocellular carcinoma (HepG2) [37]. Furthermore, a study found that galactosylated chitosan had significantly higher gene transfer efficacy in HepG2 cells than chitosan alone, and galactosylated chitosan nanoparticles had high selectivity for the liver with lower cytotoxicity [38].

2.6.2. Flow cytometry results on Bcl2, Caspase 3, 9, 8, P53, TGF-β1, and cell cycle:

The current study investigated the intrinsic pathway through the mitochondrial marker Bcl-2. The Bcl-2 and Bax proteins are grouped within a major family of proteins called "the Bcl-2 family" and represent vital apoptosis regulators. Bcl-2 can prolong cell survival by suppressing apoptosis, while Bax has the ability to improve apoptosis. Bcl2 can prevent caspase activators from being released from the mitochondria by blocking the opening of the mitochondrial permeability transition pore [39]. Table 3 showed an up-regulation of Bcl2 in the untreated group, and the percentage was 41.6±0.28%. In the CsNPs-silymarin-galactosylated group and the 5-FU group, a downregulation

of Bcl2 occurs, and the percentages were 20.5±0.278% and 26.5±0.282%, respectively. Fig. 7 showed a statistically significant decrease in BCL2 in the CsNP-silymarin-galactosylated group compared to the two groups ($p < 0.05$). As a result, we can conclude that our nanoformulated form exhibits a substantial inhibitory impact on the HepG2 cell line.

Table 3. Comparison between the galactosylated chitosan-loaded silymarin group untreated group and the 5-FU group in flowcytometry parameters:

	untreated group	**CsNPs-silymarin-galactosylated group**	**5 fluorouracil group**	**P value**
BCL2	41.6±0.28	20.5±0.278	26.5±0.282	<0.001
Caspase3	23±1.41	44.2±0.139	54.9±0.138	<0.001
Caspase9	21.1±0.14	55.9±0.142	59.6±0.28	<0.001
Caspase8	20.5±2.12	48.7±0.282	60.1±0.143	<0.001
P53	36.7±0.138	44.7±0.141	58.5±0.137	<0.001
TGFB1	28.5±0.14	50.3±0.282	59.3±0.281	<0.001

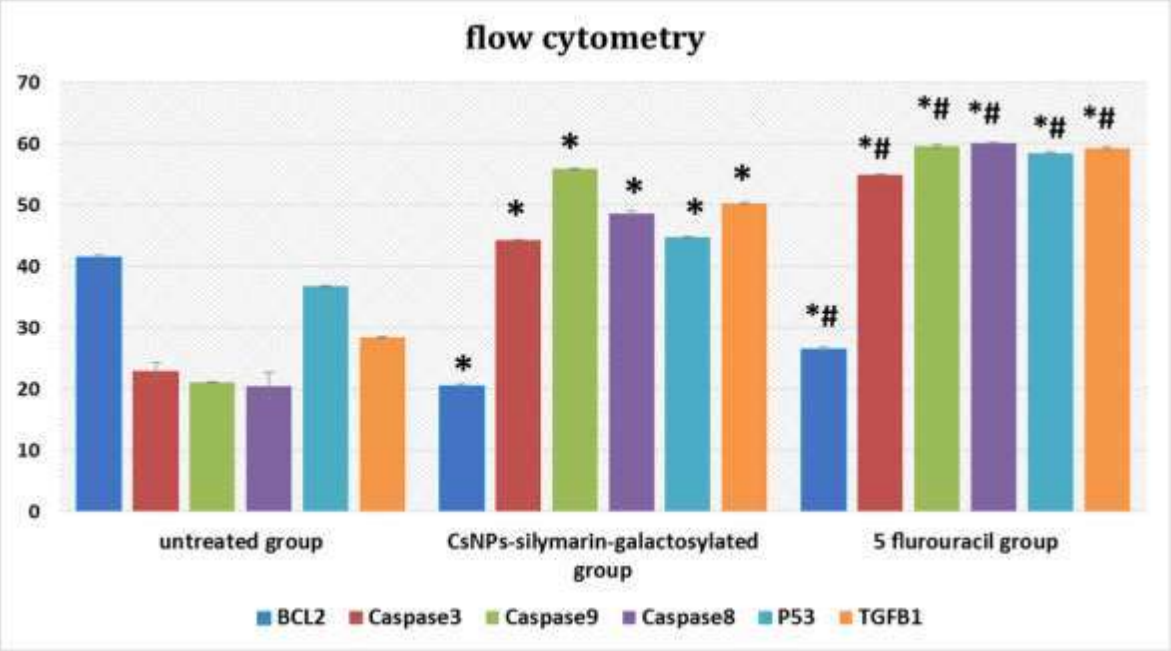

Fig.7. shows the statistical analysis of the investigated parameters. * denotes statistically significant decrease in BCL2 in the group of CsNPs-silymarin-galactosylated compared to the two groups ($p < 0.05$.) #denotes statistically significant increase in other parameters studied in the 5-fluorouracil group compared to the two groups ($p < 0.05$)

The caspase activation cascade is now being shown to be effective in imposing cell death, or apoptosis [40]. When cytochrome c leaks into the cytosol, it joins Apaf-1 and forms an apoptosome with pro-caspase-9, activating Caspase-9 [41], which is a caspase family member involved in apoptosis and cytokine processing [42]. Furthermore, activated Caspase-9 cleaves downstream caspases such as Caspase-3, which is recognized as an apoptotic executioner caspase [43]. To assess the intrinsic apoptotic pathway, the activities of executioner Caspase-3 and initiator Caspase-9 were measured. The CASP3 protein represents one of the cysteine-aspartic acid protease (caspase) family members. The successive activation of caspases plays a crucial role in the phase of cell apoptosis execution. Caspase-3 was activated in apoptotic cells through intrinsic (mitochondrial) and extrinsic (death ligand) pathways. As presented in Table 3, caspase-3 activity was cleaved after apoptotic signaling events, with percentages of 44.2±0.139% and 54.9±0.138% in the treated groups of the total number of cells. In the untreated group, the percentage of Caspase-3 was 23.0±1.41%. Fig. 7 showed a statistically significant increase in the CsNPs-Silymarin galactosylated group and in the 5-fluorouracil group compared to the untreated groups ($p < 0.05$).

The initiator Caspase 9, as shown in Table 3, showed a down-regulation in the untreated group, and the value was 21.1±0.14 %. In treated groups, galactosylated chitosan-loaded Silymarin and 5-FU upregulated Caspase-9 activity, and the percentages were 55.9±0.142% and 59.6±0.28%, respectively. Caspase-9 showed a significant increase in the CsNP-silymarin galactosylated group compared to the untreated group. Caspase-8 is a member of cysteine proteases, which are involved in apoptosis. Caspase-8 activity is an important initiator of caspase in the extrinsic pathway. Caspase-8 showed a significant increase in the CsNP-silymarin galactosylated group compared to the untreated group (Fig. 7). Intrinsic and extrinsic pathways converge at the activation of Caspase-3, a vital apoptosis executor. The P53 protein prevents tumour growth by arresting cell proliferation and triggering apoptosis. It triggers apoptosis through the activation of several pro-apoptotic genes that eventually lead to the activation of Caspase-9 and APAF-1 through various pathways [44]. Table 3 showed that p53 decreased in the untreated group, and the percentage was 36.7±0.138%. In the treated groups, the percentage of p53 became 44.7±0.141% in the group treated with CsNP-Silymarin galactosylated and 58.5±0.137 % in the 5-FU group. Statistically significant increase in the treated groups compared to the untreated group ($p <0.05$) as in Fig. 7.

TGF-β1 represents a member of the polypeptide that belongs to the transforming growth factor beta family of cytokines. This TGF-β1 is a secreted protein and has several cellular functions, such as controlling cell differentiation, cell proliferation, cell growth, and apoptosis. Table 3 showed that the percentage of TGF-β1 in the untreated group was 28.5±0.14% and that there was an overexpression of TGF-β1 in the group treated with CsNPs-Silymarin galactosylated with a percentage of 50.3±0.282%. In the group that was treated with 5-FU, the percentage of TGF-β1 was 59.3±0.281%. These findings are consistent with a previous study that used exogenous TGF- β1 on the HepG2 cell line. They found that there was an inhibition in HepG2 cell line growth, and they reported that cells had been arrested in the G1 phase, and the percentage of cells in the G2 and S phases was reduced in the group that was treated with the exogenic TGF-β1 group [45].

Table 4. Comparison between the untreated group of galactosylated chitosan-loaded silymarin group and the 5-FU group in cell cycle analysis:

	untreated group	**CsNPs-silymarin-galactosylated group**	**5 fluorouracil group**	**P value**
G0⁄G1	67.7±0.14	75.4±2.83	73.1±1.41	0.051
S phase	23.7±1.41	11.6±0.57	16.3±0.42	0.002
G2/M	8.7±0.28	2.7±0.42	4.1±0.71	0.003

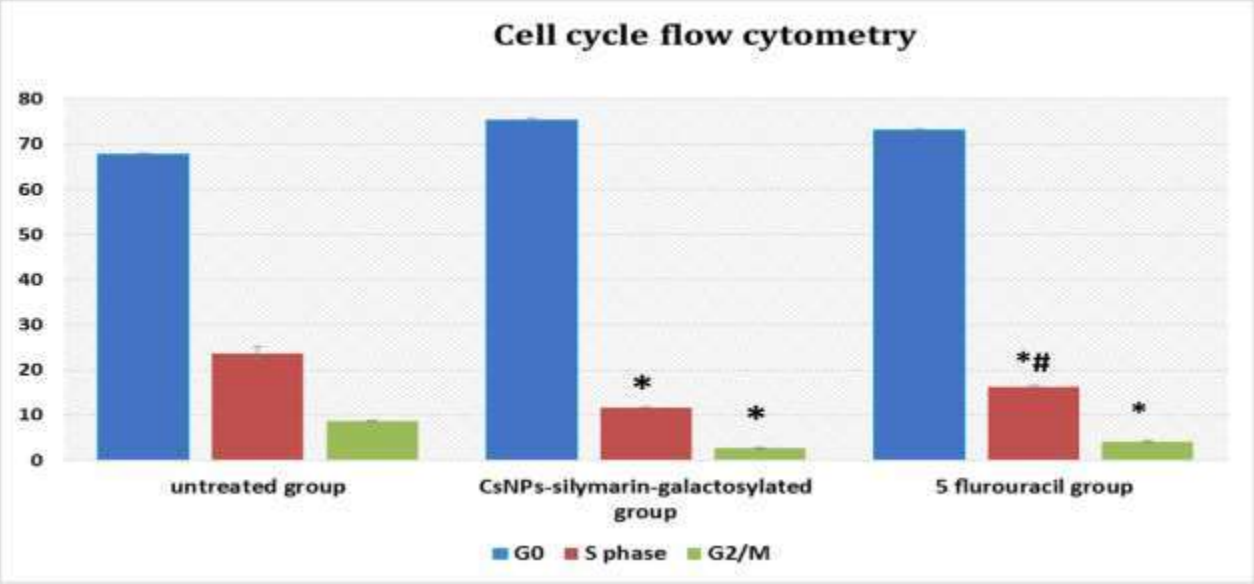

Fig.8. revealed the cell cycle analysis of the investigated parameters. No statistically significant difference in the phase G0 between the studied groups ($p > 0.05$) Statistically significant decrease in phase s in the group galactosylated with CsNP silymarin compared to the two other groups($p<0.05$). Statistically significant decrease in the G2M group in both treated groups compared to the untreated group ($p<0.05$)

The search for novel cancer-fighting therapeutics requires good integration and consideration of the cell cycle and apoptosis. Flow cytometry is an approach to distinguish different cell cycle stages (G0/G1 versus S versus G2/M), depends on a measurement method of DNA content, and was known as a single time point ("snapshot") cell measurement; it is univariate, relying solely on the determination of cellular DNA content [46]. According to Table 4, 67.7±0.14% of untreated HepG2 cells were in the G0/G1 phase, 23.7±1.41% in the synthesis phase, and 8.7±0.28% in the G2/M phase. The 5FU that was considered a positive control showed 73.1±1.41% for the G0/G1 phase,

16.3±0.42% for synthesis and 4.1±0.71% for the G2/M phase. The most potent anticancer effect was shown in our nanoformulated form, which reduced the synthesis phase to 11.6±0.57% and blocked 2.7±0.42% of the cell population in the G2/M phase. Fig.8. did not show statistically significant differences in the G0–G1 phase between the studied groups ($p > 0.05$). The same figure revealed a statistically significant decrease in phase S in the group galactosylated with CsNPs silymarin compared to the two other groups ($p < 0.05$). There was a statistically significant decrease in the G2M group in both treated groups compared to the untreated group ($p < 0.05$). As a result, we can conclude that the galactosylated CsNPs of silymarin reveal a momentous inhibitory impact on the HepG2 cell line.

2.6.3. ELISA immunoassay results of Cytochrome–c and ROS:

According to previous research, reactive oxygen species are found in small amounts in normal cells and play an important role, but are abundant in cancer cells due to the high rate of metabolic reactions [47]. Extreme ROS may induce apoptosis through the intrinsic and extrinsic pathways. Table 5 demonstrated that elevated ROS levels can inhibit tumor growth in treated groups, such as the CsNPs-Silymarin galactosylated group, which had a ROS value of 130%, and the 5-FU group, which had a value of 175%. So, we can conclude a significant increase in ROS in the CsNPs-Silymarin-galactosylated group compared to the untreated group; the percentage of reactive oxygen species reached 94%.

Table 5. Comparison between the untreated group of galactosylated chitosan-loaded silymarin group untreated group and the 5-FU group in cytochrome c and reactive oxygen species:

Sample	**ROS**		**C.C**	
	OD	**%**	**OD**	**%**
Coupled	0.656	130	0.784	9
5fu	0.828	175	0.994	13
Untreated	0.406	94	0.555	4
	U/ml		ng/ml	

Throughout apoptosis, ROS were shown to be generated through the mitochondrion, increasing the permeability of the mitochondrial membrane and causes the apoptotic phenotype [48]. Galactosylated chitosan treated HepG2 cells showed a momentous increase in ROS intensity in a dose-dependent manner compared to untreated cells. Elevated ROS production in cells induces oxidative stress, which consequently persuades the action of a cascade of reactive oxygen detoxification systems. Here, silymarin treatment considerably reduced the mitochondrial membrane potential of HepG2 cells and therefore persuaded the opening of mitochondrial permeability transition pores. The mitochondrial intermembrane space encompasses a diverse class of proteins with a distinctive release that induces cell death. Cyt c is the first molecule of this class of pro-apoptotic proteins. It can be released into the cytosol upon apoptotic stimuli and promotes the activation of caspase, which consequently induces cell demise. Mitochondrial

membrane permeabilization (MMP) is required to release apoptotic Cyt c and is considered a "point of no return" in the process of cell demise [49,50].

The existing research used an ELISA immunoassay to estimate cytochrome c release. In correlation with previous studies with silymarin conducted on other kinds of cancer cells [51,52], as reported in table (5), the results revealed that the levels of cytochrome c increased in the treated groups; In the group treated with CsNP-Silymarin galactosylated, the percentage of cytochrome c was 9% and the percentage of cytochrome c in the group treated with 5-FU was 13%. However, in the untreated group, the level of cytochrome c decreased and the percentage was 4%. As a result, we can conclude that the CsNPs-Silymarin-galactosylated group had a considerable increase in ROS and cytochrome c relative to the untreated group.

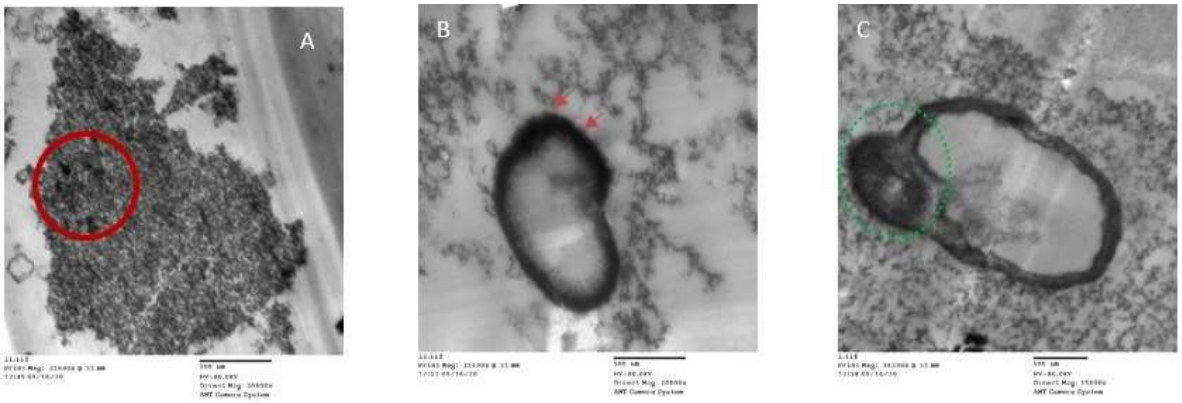

Fig.9. The high-resolution transmission electron microscope reveals the cellular uptake of the CsNPs-silymarin galactosylated formula, dark dots within the red circle (A). Accumulations of CsNP-silymarin-galactosylated particles on the outer surface of normal mitochondria (red arrows) (B). Loss of integrity of the mitochondrial membrane (green circle) (C).

Cell uptake of the formula was evaluated and we suspected that uptake was through receptor-mediated endocytosis, as shown in Fig. 9A (red circle). Mitochondria are membrane-bound cells; their potential is saved in adenosine triphosphate (ATP). The high-resolution TEM image in Fig. 9 B focused on the mitochondrion organelle, revealing the accumulations of the CsNPs-Silymarin galactosylated particles on the outer surface of mitochondria (red arrows). While the TEM image (Fig. 9 C) showed that the size, shape, and integrity of the mitochondria were lost (green circle), our hypothesis was that the investigated formula arrested HepG2 cells by suppressing mitochondrial synthesis, stimulating mitochondrial fission, and altering mitochondrial function. To the best of our knowledge, this report may be the first to investigate the potential of silymarin-loaded chitosan nanocomplexes in the treatment of hepatocellular carcinoma. However, the exact mechanism by which this silymarin-loaded chitosan nanocomplex targets overexpressed asialoglycoprotein receptors on the surface of hepatocellular carcinoma cells has not been clearly studied. Currently, we are working on studying this silymarin-loaded chitosan nanocomplex mechanistic pathway on different liver cancer cell lines to ensure its potential as an anticancer agent, parallel with screening on

normal cell lines to ensure its safety. Furthermore, these findings should be validated in vivo, since this study is a single-center experience that should be validated in other centers as a preclinical study. Our future work will focus on the cellular uptake mechanism of the investigated nanocomplex and the different pathways' effects. Furthermore, we will examine ASGPR expression patterns and levels in the normal liver and in the different grades of HCC of patients with early and advanced HepG2, taking advantage of tissue microarray technology to probe a relatively large sample size.

3. Conclusions

The poor prognosis of HCC is still a challenge and a cornerstone of attention. Targeting surface receptors is one of the essential research questions. Our goal was to direct silymarin missiles to target ASGP-R that occurs on the surface of normal hepatocytes and is overexpressed on the surface of the HCC cell. We formulated and characterized a nanoformula of CsNPs-Silymarin-galactosylated. The main finding was that homing silymarin significantly increased the expression of pro-apoptotic proteins, such as p53, in the coupled group while decreasing anti-apoptotic proteins such as Bcl-2. In our formula, the Caspase 3 and 8 values were 44.2, 48.7, and 55.9. We have found that each caspase has a distinct role in apoptosis. This means that the caspases involved in the breakdown of proteins after cytochrome c is released need to cooperate to successfully perform all parts of apoptosis. The MTT assay and the morphological changes suggested that the gallactosylated CsNPs of silymarin exhibited enhanced anticancer activity against HepG2 cells compared to silymarin nanoparticles loaded with silymarin and chitosan, where the dose of our formula was less than 250 µM. The determinations revealed that galactose could enhance uptake through the mechanism of galactose-specific receptor-mediated endocytosis and the cytotoxic ability of CsNPs-Silymarin-galactosylated nanoparticles to reach HepG2 cells. The evidence from this study suggests that the investigated formula has the potential to improve the prognosis of HCC through active targeting.

Funding

The authors have no affiliation with any organization with a direct or indirect financial interest in the subject matter discussed in the manuscript. The standing research paper was maintained through individual funding.

Consent for publication

The authors approved this version of the manuscript for publication.

Availability of data and material

The authors emphasize the availability of data and materials.

Competing Interests

The authors declared that they had no competing interests.

This manuscript has not been submitted to, nor is under review in, another journal or other publishing venue.

Ethics approval and consent to participate

The authors followed the ethics of research, approved and consented to participate in this study.

Data Sharing Statement

The authors emphasize the availability of data and materials

Authors' Contributions

Ahmed A. G. El-Shahawy and Ahmed Nabil conceived the idea. Ahmed A. G. El-Shahawy, Amr Sayed, Mariam Elwan, and Ahmed Nabil participated in the study design. Amr Sayed, Islam S. Ali, Mariam Elwan, and Zeinab Reyd prepared the materials. Ahmed A. G. El-Shahawy, Amr Sayed, Islam S. Ali, and Ahmed Nabil analyzed and interpreted the data. Ahmed A. G. El-Shahawy, Khaled Ali Elnesr, Islam S. Ali, and Ahmed Nabil wrote the manuscript. Ahmed A. G. El-Shahawy and Ahmed Nabil revised the manuscript. All authors approved the final version to be published and agreed to be responsible for all aspects of the work in ensuring that questions related to the accuracy or integrity of any part of the work are appropriately investigated and resolved.

Acknowledgements

The authors are grateful to all members of Materials Science and Nanotechnology Dept., Faculty of Postgraduate Studies for Advanced Sciences (PSAS), Beni-Suef University Egypt for supporting the preparation of the nanomaterials. Also, all members at Central Laboratory for Characterization

References

1. H. B. El-Serag and K. L. Rudolph, Gastroenterology, 2007, 132, 2576-2557.

2. Y. Pan, H. Chen and J. Yu, Biomedicines, 2020, 8, 576.

3. M. Ikeda, S. Mitsunaga, I. Ohno, Y. Hashimoto, H. Takahashi, K. Watanabe, K. Umemoto and T. Okusaka, Diseases, 2015, 3, 360–81.

4. J. I. Hare, T. Lammers, M. B. Ashford, S. Puri, G. Storm and S. T. Barry, Adv. Drug Deliv, 2017, 108, 25–38.

5. U. K. Marelli, F. Rechenmacher, T. R. Sobahi, C. Mas-Moruno and H. Kessler, Front Oncol., 2013, 3, 222.

6. G. K. Abou-Alfa, L. Schwartz, S. Ricci, D. Amadori, A. Santoro, A. Figer, J. De Greve, J. Y. Douillard, C. Lathia, B. Schwartz and I. Taylor, J. Clin. Oncol., 2006, 24, 4293–4300.

7. M. Kudo, O. Matsui, N. Izumi, H. Iijima, M. Kadoya, Y. Imai, T. Okusaka, S. Miyayama, K. Tsuchiya, K. Ueshima and A. Hiraoka, Liver Cancer, 2014, 3, 458–68.

8. Y. Yu, Z. Kovacevic and D. R. Richardson, Cell Cycle, 2007, 6, 16, 1982-94.

9. P. D. Sykes, J. P. Neoptolemos, E. Costello and C. M. Halloran, Expert Rev Gastroenterology Hepatol, 2012, 6, 343–56

10. F. Alexis, J. W. Rhee, J. P. Richie, A. F. Radovic-Moreno, R. Langer and O. C. Farokhzad, Urol Oncol., 2008, 26, 74–85

11. L. H. Reddy and P. Couvreur, J Hepatol, 2011, 55, 1461–6.

12. X. Yue, Q. Zhang and Z. Dai, Adv. Drug Deliv. Rev., 2017, 115, 155–170.

13. L. Anand Raj, R. Jonisha, B. Revathi and E. Jayalakshmy, J. Appl. Pharm. Sci., 2015, 5, 7, 001-005.

14. S. Alam, Z. Khan, G. Mustafa, M. Kumar, F. Islam, A. Bhatnagar and F. J. Ahmad, International Journal of Nanomedicine, 2012, 7, 5705–5718.

15. M. Meghreji, A. Moin, C. N. Patel, J. B. Dave, R. Badmanaban and J. A. Patel, J. Chem. Pharm. Res., 2010, 2, 1, 396-400

16. N. Tamilselvan and C. V. Raghavan, J. Young Pharm., 2015, 7, 1, 28.
17. O. A. Ghosheh, A. A. Houdi and P. A. Crooks, J Pharm Biomed Anal., 1999, 19, 757–762.

18. A. A. G. El-Shahawy, N. Elnagara, M. Zohery, M. S. Abd Elhafeez and S. I. El-Deka, International journal of polymeric materials and polymeric biomaterials, 2022, 71, 12, 910-22.

19. K. M. Iris, D. C. Tsang, S. S. Chen, L. Wang, A. J. Hunt, J. Sherwood, K. D. Vigier, F. Jérôme, Y. S. Ok, C. S. Poon, Bioresource technology, 2017, 245, 456-62.

20. P. Pozarowski and Z. Darzynkiewicz, Methods in Molecular Biology, 2004, 281, 301–311, 811-0:301.

21. M. Abdel Aziz, N. Safwat and B. Amin, The Egyptian Society of Experimental Biology, 2018, 14, 1, 133–142.

22. C. Chiu, T. Yeh, C. Lu, Y. Huang, Y. Cheng, Y. Huang, Y. Weng, Y. Liu, S. Lai, Y. Chen, Y. Chen, C Chen, H. Chen, Y. Lin and H. Wang, Oncotarget., 2017, 8, 45, 79046–79060.

23. Y. Chan, Singapore Med. J., 2003, 44, 391-396.

24. S. C. Dey, M. Al-Amin, T. U. Rashid, Z. Sultan, M. Ashaduzzaman, M. Sarker, S. Shamsuddin, IJLRET, 2016, 2, 2, 52–62.

25. S. M. Londoño-Restrepo, R. Jeronimo-Cruz, B. M. Millán-Malo, E. M. R. Muñz and M. E. Rodriguez-García, scientific Reports, 2019, 9, 5915.

26. J. Xu, G. Reiter and R. G. Alamo, Crystals, 2021, 11, 304.

27. M. B. Mohamed, Int J Appl Ceram Technol., 2020, 17, 822–830.

28. A. Abdel-Moneim, A. El-Shahawy, A. I. Yousef, S. M. Abd El-Twab, Z. E. Elden and M. Taha, International

Journal of Biological Macromolecules, 2020, 154, 1496–1504.

29. I. M. Saiyyad, D. Bhambere and S. Kshirsagar, Asian J. Pharm. Tech., 2017, 7, 4.

30. S. Gatard, M. N. Nasir, M. Deleu, N. Klai, V. Legrand and S. Bouquillon, Molecules, 2013, 18, 6101-6112.

31. A. E. Muruato, C. R. Fontes-Garfias, P. Ren, M. A. Garcia-Blanco, V. D. Menachery, X. Xie and P. Shi, Nat Commun., 2020, 11, 1, 4059.

32. Z. Ye, X. Jiang and Z. Wang, journal of software, 2012, 7, 10.

33. S. K. V. Kumar, P. R. Devi, S. Harish and E. Hemananthan, IET Nanobiotechnol., 2017, 11, 1, 104–112.

34. A. Sharma, V. Puri, V. Kakkar and I. Singh, J. Funct. Biomater., 2018, 9, 52.

35. E. Yurtcu, O. D. Iseri and F. I. Sahin, JBUON, 2015, 20, 2, 555-561.

36. K. T. Shen, M. H. Chen, H. Y. Chan, J. H. Jeng and Y. J. Wang, Food and Chemical Toxicology, 2009, 47, 8, 1864-71.

37. K. Azuma, S. Ifuku, T. Osaki, Y. Okamoto and S. Minami, Journal of Biomedical Nanotechnology, 2014, 10, 10, 891-2920.

38. M. C. Bonferoni, E. Gavini, G. Rassu, M. Maestri and P. Giunchedi, Nanomaterials, 2020, 10, 870.

39. R. M. Kluck, E. Bossy- Wetzel, D. R. Green and D. D. Newmeyer, Science, 1997, 275, 1132– 1136.

40. L. D. Osellame, T. S. Blacker and M. R. Duchen, Best Practice & Research Clinical Endocrinology & Metabolism, 2012, 26, 6, 711–723.

41. J. Li and J. Yuan, Oncogene, 2008, 27, 6194–6206.

42. S. Yuan, X. Yu, J. M. Asara, J. E. Heuser, S. J. Ludtke and C. W. Akey, Structure, 2011, 19, 8, 1084–1096.

43. M. Brentnall, L. Rodriguez-Menocal, R. L. De Guevara, E. Cepero and L. H. Boise, BMC Cell Biology, 2013, 14, 1.

44. I. Kitazumi and M. Tsukahara, The FEBS Journal, 2011, 278, 3, 427–441.

45. X. Wang, Z. Chen, R. Xu, C. Lv, J. Liu and B. Du, Oncol Lett., 2017, 13, 5, 3239–3246.

46. S. Jin and A. J. Levine, J. Cell Sci., 2001, 114, 4139– 4140.

47. K. Vermeulen, Z. N. Berneman and D. R. V. Bockstaele, Cell Prolif, 2003, 36, 3, 165–175.

48. G. Y. Liou and P. Storz, Free Radical Research, 2010, 44, 5, 479–496.

49. S. K. Katiyar, A. M. Roy and M. S. Baliga, Mol. Cancer Ther., 2005, 4, 207– 216.

50. C. Garrido, L. Galluzzi, M. Brunet, P. E. Puig, C. Didelot and G. Kroemer, Cell Death Differ, 2006, 13, 1423–1433

51. G. Ramakrishna, L. L. Muzio, C. M. Elinos-Báez, S. Jagan, T. A. Augustine, S. Kamaraj, P. Anandakumar and T. Devaki, Cell Prolif, 2009, 42, 229–240.

52. A. Tyagi, R. P. Singh, C. Agarwal and R. Agarwal, Carcinogenesis, 2006, 27, 2269–2280.